BIOLOGICAL CRYSTALLOGRAPHY

ISSN 1399-0047

An alternative RNA polymerase I structure reveals a dimer hinge

Dirk Kostrewa,[a]‡ Claus-D. Kuhn,[b]‡ Christoph Engel[c] and Patrick Cramer[c]*

[a]Gene Center Munich and Department of Biochemistry, Ludwig-Maximilians-Universität München, Feodor-Lynen-Strasse 25, 81377 Munich, Germany, [b]Elite Network of Bavaria, BIOmac Research Center, University of Bayreuth, 95440 Bayreuth, Germany, and [c]Max Planck Institute for Biophysical Chemistry, Am Fassberg 11, 37077 Göttingen, Germany. *Correspondence e-mail: patrick.cramer@mpibpc.mpg.de

Received 23 April 2015
Accepted 30 June 2015

Edited by R. McKenna, University of Florida, USA

‡ These authors contributed equally.

Keywords: RNA polymerase I; dimer; hinge; connector.

PDB reference: RNA polymerase I, 4ym7

Supporting information: this article has supporting information at journals.iucr.org/d

RNA polymerase I (Pol I) is the central, 14-subunit enzyme that synthesizes the ribosomal RNA (rRNA) precursor in eukaryotic cells. The recent crystal structure of Pol I at 2.8 Å resolution revealed two novel elements: the 'expander' in the active-centre cleft and the 'connector' that mediates Pol I dimerization [Engel *et al.* (2013), *Nature (London)*, **502**, 650–655]. Here, a Pol I structure in an alternative crystal form that was solved by molecular replacement using the original atomic Pol I structure is reported. The resulting alternative structure lacks the expander but still shows an expanded active-centre cleft. The neighbouring Pol I monomers form a homodimer with a relative orientation distinct from that observed previously, establishing the connector as a hinge between Pol I monomers.

1. Introduction

Pol I synthesizes ribosomal RNA (rRNA) in all eukaryotic cells. Pol I transcription is the first step in ribosome biogenesis and its regulation underlies cell growth (Laferté *et al.*, 2006). Deregulation of Pol I transcription is connected to human disease, in particular cancer (Drygin *et al.*, 2010; Hein *et al.*, 2013). Despite its importance in biology and biomedicine, the structure of Pol I remained elusive until recently, mainly owing to the large size and complexity of the enzyme. In 2013, however, two research groups independently determined crystal structures of Pol I from the yeast *Saccharomyces cerevisiae* (Engel *et al.*, 2013; Fernández-Tornero *et al.*, 2013). These Pol I structures were virtually identical and contained all 14 polypeptide subunits of the 589 kDa enzyme.

The structure of Pol I revealed important differences from the well known structure of Pol II, the enzyme that produces messenger RNA from protein-coding genes. Firstly, the active-centre cleft was expanded and the catalytic residues in the active site at the bottom of the cleft were rearranged, indicating that the enzyme was trapped in an inactive conformation. Secondly, a novel protein element, the 'expander', was observed inside the active-centre cleft, apparently stabilizing the expanded conformation of the enzyme and occluding the template DNA-binding site. Thirdly, another novel Pol I-specific protein element, the 'connector', invaded the active-centre cleft of a neighbouring Pol I enzyme, leading to the formation of a tightly packed Pol I homodimer. This dimer was predicted to be transcriptionally inactive because the connector and the expander both need to be released from the polymerase to allow promoter DNA loading and RNA production (Engel *et al.*, 2013; Fernández-Tornero *et al.*, 2013).

The Pol I structure matched known biochemical information. Pol I was previously shown to be able to form inactive

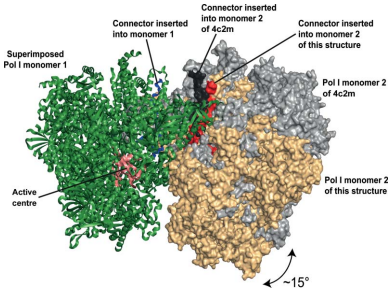

dimers (Milkereit *et al.*, 1997), whereas initiation-competent Pol I is monomeric (Blattner *et al.*, 2011; Peyroche *et al.*, 2000; Milkereit & Tschochner, 1998). Furthermore, Pol I was demonstrated to contain built-in transcription factors, namely subunit A12.2 and the A49/A34.5 subcomplex, which are partly homologous to the Pol II transcription factors TFIIS and TFIIF, respectively (Geiger *et al.*, 2010; Jennebach *et al.*, 2012). These biochemical data and the recent Pol I structures pose many new questions about the mechanism underlying Pol I transcription. For example, the expander and connector were both predicted to be mobile and to detach upon Pol I activation, but there is little information on this.

Here, we used the atomic Pol I structure (PDB entry 4c2m; Engel *et al.*, 2013) to determine the structure of Pol I in an alternative crystal form at 5.5 Å resolution. We obtained this alternative crystal form in 2005, but were only now able to solve the structure with the use of molecular replacement and the high-resolution structure of Pol I as a search model. In the alternative crystal form we observe six monomers arranged in three dimers of Pol I within one asymmetric unit. Although the overall conformation of the monomer is the same as in the previous Pol I structures, the angle between the Pol I monomers in the dimer differs significantly. This demonstrates that the previously observed Pol I dimer is not a rigid structure but rather exhibits flexibility with respect to the relative orientation of the two monomers and establishes the connector as a flexible hinge.

2. Materials and methods

Pol I from *S. cerevisiae* was prepared as described previously (Kuhn *et al.*, 2007). Crystals were grown in 8–10%(*w*/*v*) PEG 6000, 3%(*v*/*v*) MPD, 100 m*M* HEPES pH 7.5, 300 m*M* diammonium tartrate, 3 m*M* TCEP at room temperature. Crystallization screens were set up using the hanging-drop vapour-diffusion technique and a 1:1 ratio of protein and precipitant solutions. Initial microcrystals were used as a basis for streak-seeding with a cat whisker into freshly prepared drops with 9%(*w*/*v*) PEG 6000 that had been equilibrated for 3 h. The obtained crystals were rod-shaped or needle-shaped and were up to 400 µm in length. For cryoprotection, crystals were transferred into precipitant solution containing 22% PEG 400 by increasing the PEG 400 concentration in 5% increments with 1 h equilibration time per increment. Powdered W_{18} cluster compound was then added to the cryosolution and the crystal tray was transferred to 4°C inside a styrofoam box and soaked for 2 d at 4°C in the presence of the W_{18} compound followed by flash-cooling without back-soaking of the crystals. W_{18} soaking was essential for improving crystal order since it dramatically reduced the crystal mosaicity. However, defined anomalous signal from stably bound W_{18} clusters was not observed. Diffraction data were collected on beamline PXI (X06SA) of the Swiss Light Source, Villigen, Switzerland. The data were processed with *XDS* and scaled with *XSCALE* (Kabsch, 2010). Self-rotation functions were calculated with *GLRF* (Tong, 1993). The native Patterson function was calculated with the *FFT* program from the *CCP*4 suite (Winn *et al.*, 2011). Molecular replacement was carried out with *Phaser* (Read, 2001), using the first monomer of the high-resolution Pol I crystal structure with PDB code 4c2m as a search model (Engel *et al.*, 2013). The model was subjected to DEN refinement (Schröder *et al.*, 2010) using the *phenix.den_refine* module of the *PHENIX* suite (Adams *et al.*, 2010). Refinement was carried out using three TLS groups per monomer (core module, shelf module and stalk; see Fig. 4 in Engel *et al.*, 2013), one group *B* factor per residue, Cartesian NCS restraints between the six monomers, secondary-structure restraints, torsional dynamics with 600 steps between a starting temperature of 600 K and a final temperature of 300 K, and a nondeformable reference structure (γ = 0; Schröder *et al.*, 2010). Model building with *Coot* (Emsley *et al.*, 2010) was limited to shortening and repositioning of protruding flexible loops and termini, mainly using both monomers of the high-resolution Pol I crystal structure as a template (Engel *et al.*, 2013), An exception to this rule was loop 72–78 and the neighbouring residues of the Pol I subunit A34.5, which were modelled according to PDB entry 4c3i (Fernández-Tornero *et al.*, 2013). We refrained from further model adjustments because of the limited resolution of 5.5 Å. The final DEN refinement produced an *R* factor of 0.196 and a free *R* factor of 0.236, with very good stereochemistry given the limited resolution (Table 1). All structural superpositions were carried out with the *CCP*4 program *GESAMT*. Structural figures were prepared with *PyMOL* (v.1.3r1; Schrödinger).

Table 1
Crystallographic data and refinement statistics.

Values in parentheses are for the highest resolution shell.

Data processing	
Space group	*C*2 [No. 5]
Unit-cell parameters (Å, °)	a = 619.5, b = 306.6, c = 251.8, α = 90, β = 97.5, γ = 90
Resolution range (Å)	50–5.5 (5.64–5.50)
No. of observed reflections	917214
No. of unique reflections	149610
Completeness (%)	98.9 (91.0)
$\langle I/\sigma(I)\rangle$	6.6 (2.5)
$R_{\rm merge}$ (%)	22.4 (59.7)
Refinement	
No. of protein atoms	204191
No. of zinc ions	42
R factor	0.196
$R_{\rm free}$	0.236
R.m.s.d., bond lengths (Å)	0.014
R.m.s.d., bond angles (°)	1.4
Ramachandran plot	
Preferred (%)	81.0
Allowed (%)	12.5
Outliers (%)	6.5

3. Results and discussion

3.1. Alternative crystal form of Pol I

During the first years of our extensive trials to solve the Pol I crystal structure, we could crystallize the purified, endogenous *S. cerevisiae* Pol I enzyme in a crystal form that was

generally ordered after W_{18} treatment yet was poorly reproducible. After dozens of purifications and crystallization trials with very limited protein material, we eventually obtained crystals that diffracted to around 5 Å resolution. With the use of synchrotron radiation, we could collect a nearly complete diffraction data set to 5.5 Å resolution (Table 1). The unit cell of these crystals was very large, indicating that several copies of the Pol I complex were present in the asymmetric unit.

By applying Matthew coefficient probability calculations and assuming a standard solvent content (Kantardjieff & Rupp, 2003), we estimated the number of Pol I complexes in the asymmetric unit to range between six and ten (Fig. 1). A self-rotation function showed a peak for a sevenfold rotational noncrystallographic symmetry (NCS) axis along the crystallographic *c* axis and peaks for six twofold rotational NCS axes perpendicular to the crystallographic *c* axis (Fig. 2). However, a native Patterson function did not show a significant off-origin peak, arguing against the presence of translational NCS. Thus, from the estimated solvent content, the sevenfold NCS in the self-rotation function and the six noncrystallographic twofold axes plus the crystallographic twofold axis, we expected seven monomers in the asymmetric unit, forming either a ring-like arrangement or a helical structure.

3.2. Crystal structure determination

Despite the extensive NCS present in this crystal form and the possibility of NCS averaging, we could not phase the structure by molecular replacement using either the homologous Pol II structure or the cryo-EM structure of *S. cerevisiae* Pol I (Kuhn *et al.*, 2007). Only when the atomic model of Pol I became available were we able to successfully perform molecular replacement with *Phaser* (Read, 2001). In particular, we used the first monomer of the high-resolution crystal structure of the Pol I dimer (chains *A*–*O* of PDB entry 4c2m; Engel *et al.*, 2013) as a search model after having removed flexible surface regions. *Phaser* found six Pol I monomers in the asymmetric unit, which we rearranged into three dimers. The resulting model was manually adjusted in *Coot* (Emsley *et al.*, 2010) and subjected to DEN refinement (Schröder *et al.*, 2010) as implemented in *PHENIX* (Adams *et al.*, 2010). The final structure is of good quality, with *R* and $R_{\rm free}$ factors of 19.6 and 23.6%, respectively, and reasonable stereochemistry (Table 1).

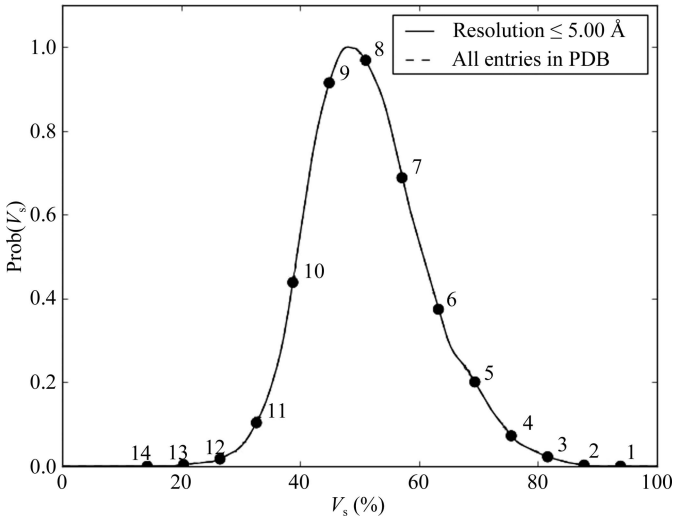

Figure 1
Estimated solvent content and number of Pol I copies in the asymmetric unit. Calculated using the web applet *MATTPROB* (Kantardjieff & Rupp, 2003) with the 2013 kernel estimator. The dashed curve for all PDB entries is hidden behind the solid curve.

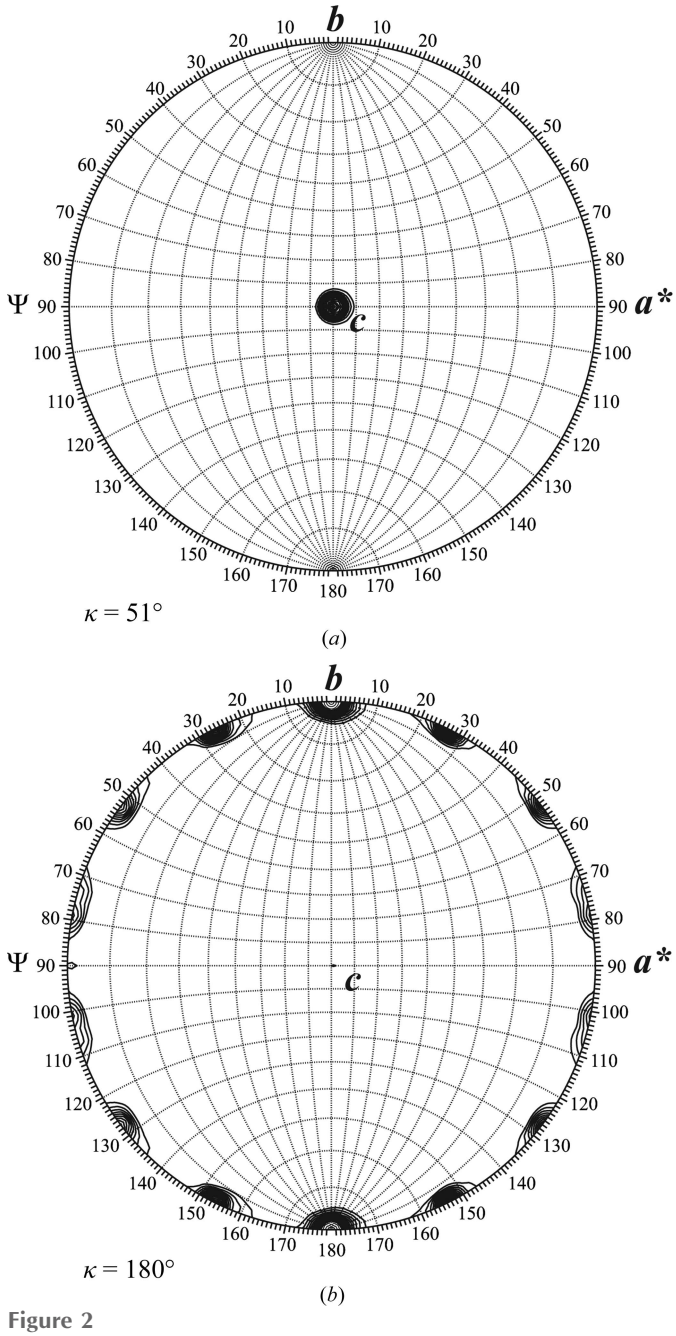

Figure 2
Self-rotation functions calculated with *GLRF* (Tong, 1993). (*a*) The section at $\kappa = 51^\circ$ shows a strong peak for a sevenfold noncrystallographic symmetry axis along the crystallographic *c* axis. (*b*) The section at $\kappa = 180^\circ$ shows strong peaks for six twofold noncrystallographic symmetry axes perpendicular to the crystallographic *c* axis.

Table 2
Superpositions of six crystallographically independent Pol I monomers.

The r.m.s.d. values are given in Å and the number of aligned C^{α} atoms is given in parentheses. M1 refers to the first monomer of the crystal structure presented here. 4c2m M1 and 4c2m M2 refer to the two monomers of the crystal structure reported by Engel *et al.* (2013). 4c3h, 4c3i and 4c3j refer to the monomers of the structures reported by Fernández-Tornero *et al.* (2013).

	4c2m M1	4c2m M2	4c3h	4c3i	4c3j
M1	1.19 (4244)	1.20 (4238)	1.18 (4175)	1.07 (4176)	1.05 (4177)
4c2m M1	—	0.61 (4307)	0.78 (4195)	0.95 (4161)	0.88 (4199)
4c2m M2	—	—	0.80 (4147)	0.88 (4135)	0.80 (4169)
4c3h	—	—	—	0.63 (4315)	0.54 (4355)
4c3i	—	—	—	—	0.25 (4315)

3.3. Unusual crystal packing and overall structure

Given that our initial NCS analysis suggested sevenfold symmetry, the presence of only six Pol I monomers in the asymmetric unit was surprising. However, the unusual crystal packing could explain this discrepancy because six Pol I monomers were arranged into three Pol I dimers, forming a pseudo-heptagonal helix together with their crystallographic symmetry equivalents along the crystallographic *c* axis (Fig. 3). This arrangement explains the observed sevenfold NCS peak along with the six twofold NCS axes perpendicular to *c* (Fig. 3). The pseudo-heptagonal helix is repeated by a crystallographic translation, forming continuous protein tubes that pack in the crystallographic *ab* plane and leave a slit along the crystallographic *c* axis (Fig. 4). The six Pol I monomers are virtually identical, with r.m.s.d. values of 0.33 ± 0.06 Å for all common C^{α} atoms, consistent with the use of NCS restraints during refinement. Comparison of the six monomers of this alternative Pol I structure to both high-resolution structures of Pol I (Engel *et al.*, 2013; Fernández-Tornero *et al.*, 2013) unveils a high degree of similarity, as demonstrated by r.m.s.d. values for C^{α} atoms in the range 0.7–1.1 ± 0.2 Å (Table 2). Thus, considering the resolution of our data, we conclude that there is no significant difference in the overall structure of the Pol I monomers in the three available crystal forms.

3.4. Mobility of the expander element

In the alternative Pol I structure presented here, the expander is absent from the active-centre cleft of all six Pol I monomers. The high mobility of the expander was already apparent in the initial, model-biased electron-density map obtained after molecular replacement, in which negative difference density was observed for the expander. In addition, omitting the expander during refinement did not return any interpretable electron density in an OMIT map. To exclude the possibility that model bias dominated the OMIT map at the limited resolution of the data set, we tested whether the

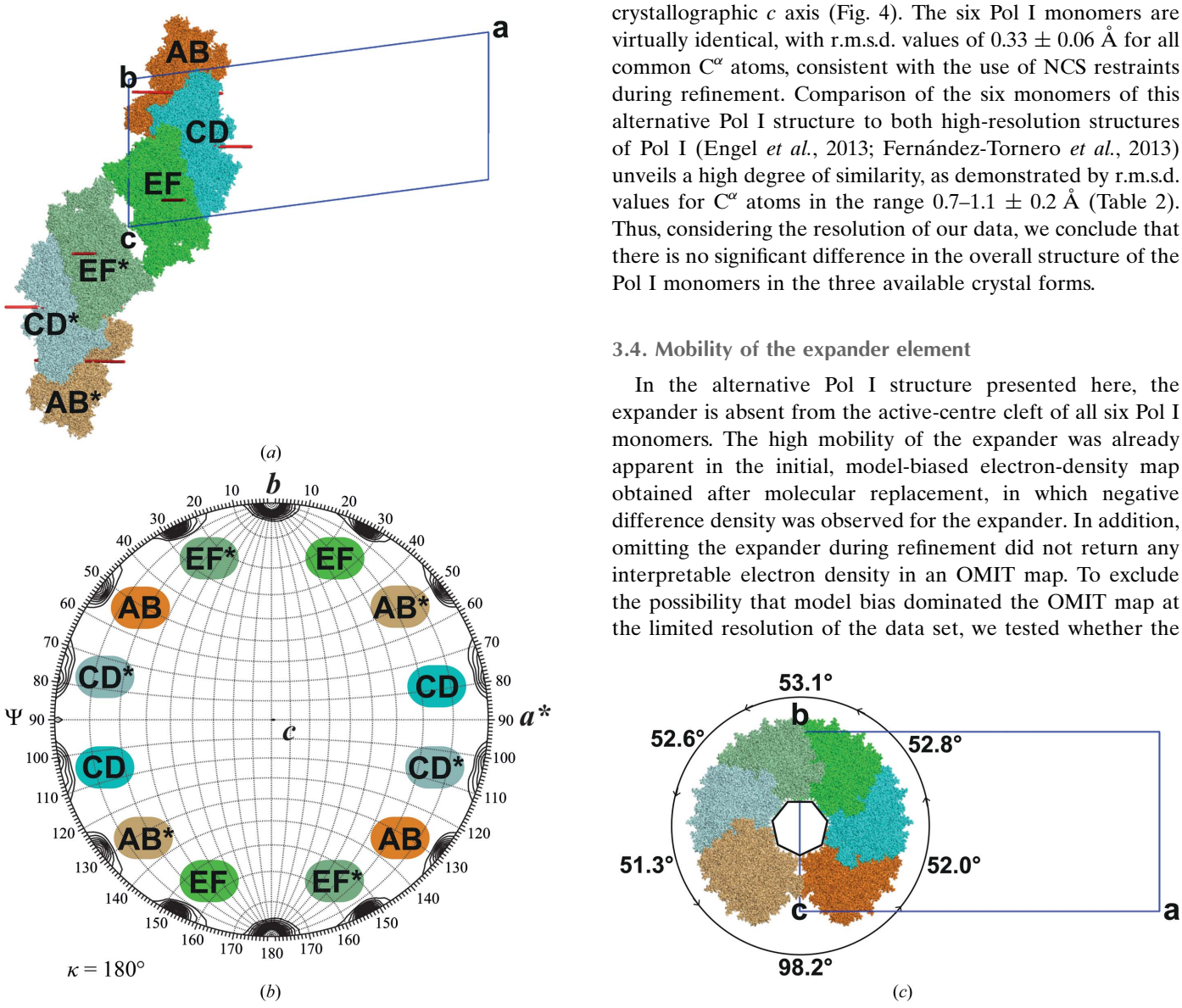

Figure 3
Packing of Pol I dimers within the crystal. (*a*) Helical arrangement of the *AB* (orange), *CD* (cyan) and *EF* (green) dimers along the crystallographic *c* axis and their symmetry equivalents through a crystallographic twofold axis along *b*: *AB** (pale orange), *CD** (pale cyan) and *EF** (pale green). The noncrystallographic twofold axes of all dimers are shown as sticks in red. The unit cell is shown in blue and labelled with *a*, *b*, *c*. (*b*) The section at $\kappa = 180^{\circ}$ of the self-rotation function, as in Fig. 2(*b*), with the peaks for the noncrystallographic twofold axes of the *AB*, *CD* and *EF* dimers and their symmetry equivalents *AB**, *CD** and *EF** labelled and coloured as in (*a*). (*c*) View of the helical packing along the crystallographic *c* axis. The dimers are coloured as in (*a*). The pseudo-heptagonal arrangement along the *c* axis is symbolized by a black heptagon in the hole of the helical arrangement. Black curved arrows indicate the relative rotation between adjacent dimers with their respective rotation angles. The unit cell is depicted as in (*a*).

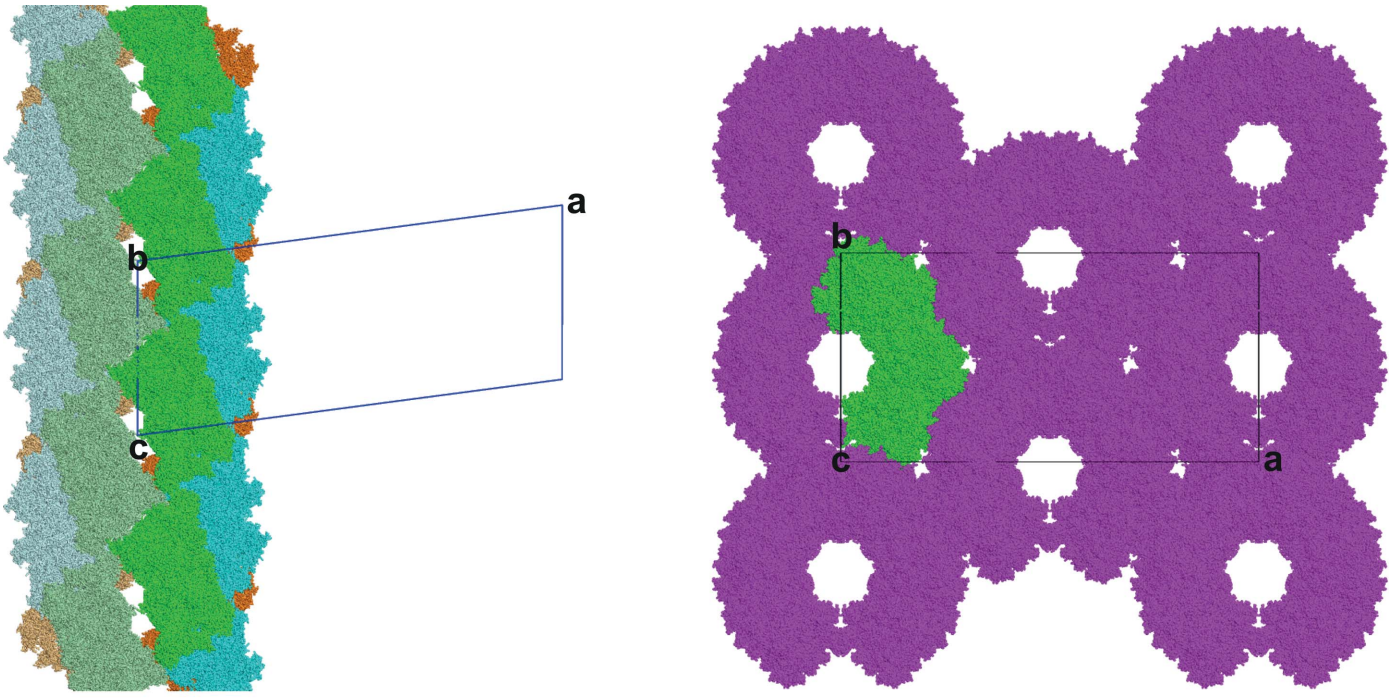

(*a*) (*b*)

Figure 4
The helical arrangement of the dimers in the crystals results in continuous tubes. (*a*) View along the crystallographic *b* axis showing one continuous tube formed by dimers and their symmetry equivalents along the *c* axis. The colours are the same as in Fig. 3. The unit cell is shown in blue and is labelled with *a*, *b*, *c*. (*b*) View along the crystallographic *c* axis showing close packing of the continuous tubes in (*a*) and their symmetry equivalents in the *ab* plane. The asymmetric unit with three dimers *AB*, *CD* and *EF* is coloured green; symmetry equivalents are coloured magenta. The unit cell is shown in black and labelled with *a*, *b*, *c*.

omission of the well defined connector helix from refinement would return electron density. In contrast to the expander, clear electron density for all six copies of the connector was returned in the resulting OMIT map (Fig. 5*a*). Taken together, we conclude that the expander is mobile in our alternative Pol I crystal structure and we therefore removed it from the model entirely. Besides a highly mobile expander, we noticed that the width of the nucleic acid-binding cleft was reduced by ∼1–2 Å compared with the three other available high-resolution Pol I monomer structures with bound expander (PDB entries 4c2m, 4c3h and 4c3j; Engel *et al.*, 2013; Fernández-Tornero *et al.*, 2013). However, the width of the nucleic acid-binding cleft is structurally very similar to the only other high-resolution Pol monomer structure with an absent expander (PDB entry 4c3i; Fernández-Tornero *et al.*, 2013).

3.5. The connector acts as a hinge between Pol I monomers

The major difference between the Pol I crystal structure reported here and the previously published high-resolution structures is a change in the relative orientation of the two Pol I monomers within a Pol I dimer (Fig. 5*b*). The angle between the Pol I monomers differs by ∼15° from that observed in the high-resolution structures. This is the case for all three Pol I dimers in the novel crystal structure, whereas the three dimers only differ by ∼1° in the relative orientation of their monomers. Notably, all previously observed Pol I dimers are highly similar, despite being present in largely different crystal lattices, with Pol I being a noncrystallographic (Engel *et al.*, 2013) or a crystallographic dimer (Fernández-Tornero *et al.*, 2013).

Despite this large difference in the relative orientation of the Pol I monomers within a dimer in our new crystal form, no significant conformational changes were observed in the dimer interface formed between the connector of one monomer and the clamp domain of the other monomer. Instead, the re-orientation of the Pol I monomers with respect to each other is apparently accommodated by changes in the mobile loop of the connector element (A43 residues 252–263). The large change in the dimer angle appears to be possible by a simple rigid-body rotation of the two Pol I monomers against each other. Thus, a change in the relative orientation of two Pol I monomers is likely to be possible without significant energy cost and might therefore result in a distribution of different dimer angles in solution. This conformational flexibility between Pol I monomers is likely to be important for the binding to and release of factors from the inactive Pol I dimer and thus transcription regulation, as suggested by Engel *et al.* (2013).

Acknowledgements

C-DK was supported by a Kekulé Fellowship from the Fonds der Chemischen Industrie (FCI) and by the Elite Network of Bavaria. CE was supported by a PhD student fellowship from the Boehringer Ingelheim Fonds, the Elite Network Bavaria program ‘Protein Dynamics in Health and Disease’ and the Graduate Research Academy ‘RNA Biology’ of SFB960.

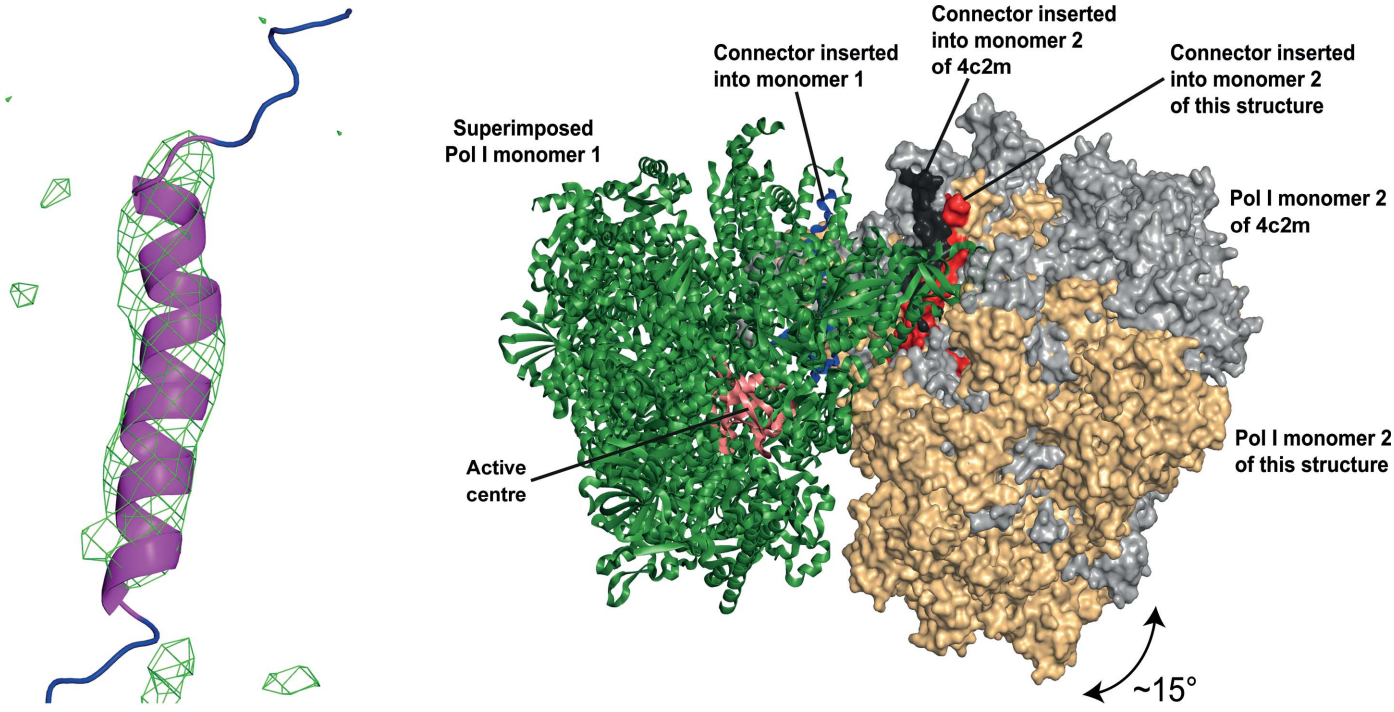

Figure 5
Alternative Pol I dimer and connector element. (*a*) The presence of the connector element. OMIT $mF_o - DF_c$ electron-density map contoured at 3 r.m.s.d. (ρ). The OMIT map is shown as a green mesh; the omitted connector α-helix is shown in ribbon representation in magenta. The loops on either side of the connector α-helix that are coloured blue were not omitted. (*b*) Altered relative orientation of the Pol I monomers in the dimer after superposition of the first monomer. The angle between the two monomers differs by ~15° between the high-resolution structure of Engel *et al.* (2013), PDB entry 4c2m, and the structure presented here. One of the first Pol I monomers is shown in a green cartoon representation. The second Pol I monomers are shown as surface representations in grey for the high-resolution structure 4c2m and in wheat for this structure. The active centre in monomer I is highlighted in salmon. The connector element inserted in monomer I is shown in blue cartoon representation; the connector elements inserted in monomer II are shown in black surface representation for the high-resolution structure 4c2m and in red surface representation for this structure.

PC was supported by the Deutsche Forschungsgemeinschaft (SFB960), the Advanced Grant 'TRANSIT' of the European Research Council and the Volkswagen Foundation. We acknowledge Stefan Jennebach, who devoted a large portion of his PhD work on obtaining improved Pol I crystals in the crystal form presented here. We thank Herbert Tschochner, Jochen Gerber and colleagues from the University of Regensburg for advice. We thank Sebastian Geiger, Claudia Blattner, Tobias Gubbey and Simon Neyer for help. Diffraction data were collected on beamline PXI (X06SA) at the Swiss Light Source in Villigen, Switzerland.

References

Adams, P. D. *et al.* (2010). *Acta Cryst.* D**66**, 213–221.
Blattner, C., Jennebach, S., Herzog, F., Mayer, A., Cheung, A. C. M., Witte, G., Lorenzen, K., Hopfner, K.-P., Heck, A. J. R., Aebersold, R. & Cramer, P. (2011). *Genes Dev.* **25**, 2093–2105.
Drygin, D., Rice, W. G. & Grummt, I. (2010). *Annu. Rev. Pharmacol. Toxicol.* **50**, 131–156.
Emsley, P., Lohkamp, B., Scott, W. G. & Cowtan, K. (2010). *Acta Cryst.* D**66**, 486–501.
Engel, C., Sainsbury, S., Cheung, A. C., Kostrewa, D. & Cramer, P. (2013). *Nature (London)*, **502**, 650–655.
Fernández-Tornero, C., Moreno-Morcillo, M., Rashid, U. J., Taylor, N. M., Ruiz, F. M., Gruene, T., Legrand, P., Steuerwald, U. & Müller, C. W. (2013). *Nature (London)*, **502**, 644–649.
Geiger, S. R., Lorenzen, K., Schreieck, A., Hanecker, P., Kostrewa, D., Heck, A. J. R. & Cramer, P. (2010). *Mol. Cell*, **39**, 583–594.
Hein, N., Hannan, K. M., George, A. J., Sanij, E. & Hannan, R. D. (2013). *Trends Mol. Med.* **19**, 643–654.
Jennebach, S., Herzog, F., Aebersold, R. & Cramer, P. (2012). *Nucleic Acids Res.* **40**, 5591–5601.
Kabsch, W. (2010). *Acta Cryst.* D**66**, 125–132.
Kantardjieff, K. A. & Rupp, B. (2003). *Protein Sci.* **12**, 1865–1871.
Kuhn, C. D., Geiger, S. R., Baumli, S., Gartmann, M., Gerber, J., Jennebach, S., Mielke, T., Tschochner, H., Beckmann, R. & Cramer, P. (2007). *Cell*, **131**, 1260–1272.
Laferté, A., Favry, E., Sentenac, A., Riva, M., Carles, C. & Chédin, S. (2006). *Genes Dev.* **20**, 2030–2040.
Milkereit, P., Schultz, P. & Tschochner, H. (1997). *Biol. Chem.* **378**, 1433–1443.
Milkereit, P. & Tschochner, H. (1998). *EMBO J.* **17**, 3692–3703.
Peyroche, G., Milkereit, P., Bischler, N., Tschochner, H., Schultz, P., Sentenac, A., Carles, C. & Riva, M. (2000). *EMBO J.* **19**, 5473–5482.
Read, R. J. (2001). *Acta Cryst.* D**57**, 1373–1382.
Schröder, G. F., Levitt, M. & Brunger, A. T. (2010). *Nature (London)*, **464**, 1218–1222.
Tong, L. (1993). *J. Appl. Cryst.* **26**, 748–751.
Winn, M. D. *et al.* (2011). *Acta Cryst.* D**67**, 235–242.